A transcription factor-sRNA-mediated double-negative feedback loop confers pathogen-specific control of quorum-sensing genes

Authors

Ameya A. Mashruwala[1,2,3], Kaitlin Decker[1,2,5], Chenyi Fei[1,2,4], Julie Valastyan[1,2], and Bonnie L. Bassler[1,2*]

Affiliations

[1]Department of Molecular Biology, Princeton University, Princeton, New Jersey 08544, USA

[2]The Howard Hughes Medical Institute, Chevy Chase, MD 20815, USA

[3]Current address: The Stowers Institute for Medical Research, Kansas City, MO, 64110

[4]Current address: Massachusetts Institute of Technology, Cambridge, MA 02139

[5]Current address: Rutgers University, Piscataway, NJ, 08854

*Correspondence to: bbassler@princeton.edu

Abstract

The cell-to-cell communication process called quorum sensing enables bacteria to synchronize collective behaviors. Quorum sensing relies on the production, release, and detection of signaling molecules called autoinducers. In *Vibrio cholerae*, the VqmA transcription factor, following binding of the DPO autoinducer, activates expression of the gene encoding the VqmR small regulatory RNA. VqmR controls traits including biofilm formation. Here, we identify repressors of DPO-VqmA-VqmR signaling. We focus on one identified repressor, the LuxT transcription factor. We show that LuxT represses *vqmR* transcription. VqmR post-transcriptionally represses *luxT* translation. This arrangement forms a double-negative feedback loop between the two regulators. Reciprocal control hinges on the N-terminal 8 amino acids of LuxT. The nucleotide sequence encoding this LuxT region serves as the VqmR binding site in the *luxT* mRNA and the amino acids specified by this same N-terminal region are required for LuxT to bind the *vqmR* promoter. This same LuxT N-terminal region also expands the DNA motifs to which LuxT can bind. We show this regulatory circuit is unique to *V. cholerae* and closely related species and absent from other vibrios. We define the set of LuxT-controlled genes in *V. cholerae* and

show that LuxT promotes biofilm formation, a key requirement for successful colonization of eukaryotic hosts.

Importance

Bacterial quorum sensing enables control of collective behaviors. In *Vibrio cholerae*, the DPO-VqmA-VqmR quorum-sensing circuit governs key processes, including biofilm formation. Here, we identify a double-negative feedback loop between the transcription factor LuxT and the small RNA VqmR. This regulatory circuit depends on an eight amino acid N-terminal region that exists only in *V. cholerae* LuxT and LuxT from its close relatives. This short peptide sequence confers three distinct functions: It enables LuxT to repress *vqmR*, renders *luxT* mRNA susceptible to VqmR repression, and governs which DNA motifs LuxT can bind. Our findings reveal a pathogen-specific regulatory module that links small RNA targeting of mRNAs to transcription factor DNA binding specificity. The results show how evolution tailors bacterial regulatory circuits to adapt to different environments.

Introduction

Quorum sensing (QS) is a process of cell-to-cell communication that bacteria use to coordinate group behaviors (1, 2). QS involves the production, release, and population-wide detection of extracellular signal molecules called autoinducers (AIs) (1, 2). At low cell density, AI concentration is below the threshold for detection and genes required to perform individual behaviors are expressed (2, 3). As population density increases, AIs accumulate and interact with their partner receptors (2–4). AI-bound receptors drive the transition from the low cell density to the high cell density gene expression pattern, and consequently, bacteria enact group behaviors (5–10). In the human pathogen *Vibrio cholerae*, the causative agent of the cholera disease, QS regulates traits including virulence factor production and biofilm formation (11–14). Regarding *V. cholerae* biofilms, they form at low cell density, and at high cell density, QS represses biofilm formation and promotes biofilm dispersal (11, 15, 16).

48 *V. cholerae* possesses multiple QS systems that operate in parallel (14, 17–21). The
49 current work focuses on the QS system that relies on the AI called DPO (3,5-
50 dimethylpyrazin-2-ol), which is produced via a threonine dehydrogenase (Tdh)-
51 dependent mechanism (18, 22). DPO is bound by the VqmA transcription factor (18). At
52 high cell density, the DPO-VqmA complex activates expression of *vqmR,* encoding the
53 VqmR small RNA (sRNA) (18, 23). VqmR post-transcriptionally regulates gene
54 expression, including repressing genes required for biofilm formation (18, 23).
55
56 In addition to extracting information encoded in DPO, VqmA also acts as an information
57 processing hub that enables *V. cholerae* to integrate cues derived from the environment
58 and the human host, such as oxygen levels and bile salts (24). VqmA indirectly perceives
59 oxygen through cysteine residues that form redox-responsive disulfide bonds. In the
60 presence of both oxygen and DPO, VqmA forms a C134-C134 intermolecular disulfide
61 bond that enhances binding to the *vqmR* promoter. Indeed, the $VqmA_{C134A}$ protein, which
62 cannot form this disulfide bond, exhibits diminished DNA binding capacity (24).
63
64 Here, we perform a genetic screen to identify additional regulators of the DPO-VqmA-
65 VqmR QS circuit. We focus on the LuxT transcription factor revealed in our analysis. We
66 define the mechanism by which LuxT represses *vqmR* expression, we show that VqmR
67 represses LuxT production, and we demonstrate how reciprocal regulation shapes QS-
68 controlled behaviors. Our assessment of the distribution of this LuxT-VqmR double-
69 negative feedback loop shows it is restricted to *V. cholerae* and its close relatives due to
70 the presence of a 24 base pair (bp) sequence in the *V. cholerae luxT* mRNA to which
71 VqmR binds, a sequence that is lacking in other vibrios (Figure 1). Our findings indicate
72 that reciprocal LuxT-VqmR regulation could provide functions specific to niches inhabited
73 by *V. cholerae*.
74
75 **Results**
76 **A genetic screen in *V. cholerae* reveals repressors of DPO-VqmA-VqmR QS signal**
77 **transduction.** QS information, cues from the local environment, and human host-derived
78 stimuli are all integrated by VqmA to modulate its transcriptional activity (24). Given this

79 understanding, we wondered whether additional inputs also regulate VqmA-directed QS
80 signaling. An earlier screen revealed that VqmA activates *vqmR* expression (23). Here,
81 we carry out the opposite screen: a transposon mutagenesis screen for repressors of
82 *vqmR*. Our strategy exploited a partially impaired VqmA protein, $VqmA_{C134A}$, that exhibits
83 reduced DNA binding capacity at the *vqmR* promoter (24). Using the $VqmA_{C134A}$ allele
84 enabled us to conduct a simple, visual blue-white colony screen using a transcriptional
85 reporter in which the *vqmR* promoter drives *lacZ* expression (hereafter P*vqmR-lacZ*, with
86 the P prefix denoting promoter). Because basal P*vqmR-lacZ* activity is low in *V. cholerae*
87 carrying $VqmA_{C134A,}$ colonies are white/pale blue, unlike *V. cholerae* colonies possessing
88 wildtype (WT) VqmA, which are bright blue (Supplementary Figure S1). We reasoned that
89 *V. cholerae vqmA*$_{C134A}$ P*vqmR-lacZ* mutants that had obtained transposon insertions in
90 genes encoding repressors of DPO-VqmA-VqmR signaling would drive higher P*vqmR-*
91 *lacZ* expression and be identifiable as blue colonies on petri plates (Supplementary
92 Figure S1). Based on this logic, we mutagenized Δ*tdh vqmA*$_{C134A\text{-}FLAG}$ P*vqmR-lacZ V.*
93 *cholerae* and screened for blue colonies in the presence of X-gal. We have previously
94 shown that the *vqmA*$_{C134A\text{-}FLAG}$ allele accurately reflects VqmA protein abundance and
95 function (24). Using a strain lacking *tdh* for the screen ensured that hits would be restricted
96 to genes encoding components that act on signal relay (*vqmA* or *vqmR*) not signal
97 production (*tdh*). We did not supply DPO during the screen. The strategy was to keep the
98 endogenous P*vqmR-lacZ* activity as low as possible to enhance detection of insertion
99 mutants exhibiting even modest increases. We assessed ~20,000 colonies and identified
100 17 mutants, representing 14 unique transposon insertion sites. The mutated genes
101 encoded 6 regulatory proteins, 4 components involved in transport and metabolism, and
102 4 genes with undefined functions.
103
104 To confirm the hits from our screen, we engineered P*vqmR-lux* as a reporter to quantify
105 *vqmR* promoter activity (23, 24). We introduced the P*vqmR-lux* fusion onto the
106 chromosomes of Δ*tdh V. cholerae* possessing either *vqmA*$_{FLAG}$ or *vqmA*$_{C134A\text{-}FLAG}$. In the
107 absence of DPO, P*vqmR-lux* activity was ~27-fold higher in the Δ*tdh vqmA*$_{FLAG}$ strain than
108 in the Δ*tdh vqmA*$_{C134A\text{-}FLAG}$ strain, showing that $VqmA_{C134A\text{-}FLAG}$ is, as expected, impaired
109 in activity. Supplementation with DPO increased *vqmR-lux* activity ~4-fold in the Δ*tdh*

110 *vqmA*$_{FLAG}$ strain and ~37-fold in the Δ*tdh vqmA*$_{C134A\text{-}FLAG}$ strain (Figure 2A, B,
111 respectively). Thus, the P*vqmR-lux* reporter responds properly to DPO-mediated VqmA
112 activation, and exploiting the VqmA$_{C134A\text{-}FLAG}$ mutant expands the dynamic range of the
113 AI response assay.
114
115 To verify that components identified in our screen influence DPO-VqmA-VqmR signaling,
116 we deleted each of the identified genes from the chromosome of the Δ*tdh vqmA*$_{C134A\text{-}FLAG}$
117 P*vqmR-lux V. cholerae* strain. Deletions of four of the candidate genes, *vc0122, vc2614,*
118 *vca0566,* and *vca0917* resulted in 9-, 13.5-, 2.8-, and 3.3-fold increases in P*vqmR-lux*
119 activity, respectively (Figure 2C; growth curves for the strains are provided in
120 Supplementary Figure S2 and the phenotypes following complementation of the deleted
121 genes are shown in Supplementary Figure S3). Some temporal differences occur across
122 strains. For simplicity, throughout this work we report maximal fold changes and OD_{600}
123 values during early-exponential growth. The remaining ten genes did not significantly alter
124 P*vqmR-lux* output (Supplementary Figure S4). It is possible that these ten genes were
125 false positives or that they only influence *vqmR* expression on solid medium, etc. We did
126 not study them further. The remainder of the present work is focused on *vc0122, vc2614,*
127 *vca0566,* and *vca0917*. These genes encode Acy, Crp, WigR, and LuxT, respectively.
128
129 **LuxT represses *vqmR* transcription.** The putative repressors identified in our screen
130 could decrease DPO-VqmA-VqmR signaling by repressing expression of either *vqmA* or
131 *vqmR*. To distinguish between these two possibilities, we engineered a Δ*tdh* Δ*vqmA V.*
132 *cholerae* strain carrying P$_{BAD}$-*vqmA* at a neutral chromosomal locus. The strain also
133 harbors the chromosomal P*vqmR-lux* fusion. We refer to this strain simply as the P$_{BAD}$-
134 *vqmA* strain. We introduced deletions of *acy*, *crp*, *wigR*, and *luxT* into the P$_{BAD}$-*vqmA*
135 strain and measured P*vqmR-lux* output. Our rationale is as follows: VqmA is required to
136 activate *vqmR* expression. In the P$_{BAD}$-*vqmA* strain, following the addition of arabinose,
137 VqmA is produced and activates P*vqmR-lux*. Since *vqmA* is driven by a synthetic
138 promoter, it is not subject to native regulation. Thus, if deletion of a gene(s) identified in
139 our screen results in increased P*vqmR-lux* activity, then *vqmR* must be the target of that
140 particular repressor. By contrast, if no change in P*vqmR-lux* occurs, then we can infer

141 that repression must occur through changes in *vqmA* transcription, VqmA activity, or
142 VqmA turnover. Figure 3A shows that deletion of *crp* and *luxT* from the P_{BAD}-*vqmA* strain
143 resulted in ~13.2-fold and 2.5-fold increases in P*vqmR-lux* activity suggesting that *crp*
144 and *luxT* modulate VqmR levels. By contrast, no change in P*vqmR-lux* activity occurred
145 when *acy* and *wigR* were deleted, suggesting they modify *vqmA* expression or VqmA
146 abundance or activity (Figure 3A; growth curves for the strains are provided in
147 Supplementary Figure S5). We quantified $VqmA_{FLAG}$ abundance in the Δ*tdh V. cholerae*
148 strain when *acy* or *wigR* was deleted. We note that, here, $vqmA_{FLAG}$ is driven by its
149 endogenous promoter. We used the Δ*tdh* Δ*crp* and Δ*tdh* Δ*luxT* strains as controls for
150 comparison. Our logic was that if Acy and WigR modify *vqmA* transcription or VqmA
151 abundance, then in the Δ*acy* and Δ*wigR* strains, VqmA levels would differ from those in
152 the parent strain. Neither mutant displayed any change in $VqmA_{FLAG}$ abundance
153 (Supplementary Figure S6). Acy and WigR could affect VqmA function; we have not
154 examined that mechanism.
155
156 For the remainder of this study, we characterize the role of LuxT in *vqmR* regulation. *V.*
157 *cholerae* LuxT (*$LuxT_{Vc}$*) is a transcription factor, the mRNA of which was previously
158 identified as a direct target of repression by the VqmR sRNA (23). Our identification of
159 $LuxT_{Vc}$ as a repressor of *vqmR* suggests that VqmR and $LuxT_{Vc}$ constitute a double-
160 negative feedback loop.
161
162 To probe whether LuxT regulates *vqmR* by transcriptional repression, we analyzed the
163 *vqmR* promoter for a consensus LuxT binding sequence. *Vibrio harveyi* LuxT ($LuxT_{Vh}$)
164 shares 75% amino acid identity with $LuxT_{Vc}$, making it likely that both proteins bind similar
165 DNA sequences. A prior study in *V. harveyi* identified a LuxT ($LuxT_{Vh}$) binding site in the
166 promoter of *qrr*1 (25). Inspection of the *V. cholerae vqmR* promoter (P$vqmR_{Vc}$) using the
167 site in the *qrr*1 promoter as a guide, revealed a potential LuxT binding site located at -28
168 to -9 upstream of the $vqmR_{Vc}$ transcriptional start site. To determine if $LuxT_{Vc}$ binds this
169 motif, we purified 6X-His-$LuxT_{Vc}$ and combined it in an electrophoretic mobility shift assay
170 (EMSA) with a probe containing *V. cholerae* P$vqmR_{Vc}$ (-111 to +49) or, as a control, the
171 same probe containing a scrambled version of the putative LuxT binding sequence

172 (P*vqmR*$_{Vc\ scrambled}$). 6X-His-LuxT$_{Vc}$ bound to P*vqmR*$_{Vc}$ but not P*vqmR*$_{Vc\ scrambled}$,
173 suggesting that LuxT directly represses *vqmR* expression (Figure 3B). We refer to the
174 LuxT binding motif in P*vqmR*$_{Vc}$ as Motif 1. Since we already know that the VqmR sRNA
175 represses *luxT*, we conclude that LuxT and VqmR interact in a double-negative feedback
176 loop.
177
178 **LuxT-VqmR feedback loops are present only in *V. cholerae* and *V. cholerae*-like**
179 **vibrio species.** Given that both LuxT and VqmR are present across vibrios, we wondered
180 whether their regulatory interactions are likewise conserved across the genus. Using
181 bioinformatic analyses, we compared the DNA sequences encoding P*vqmR* and the *luxT*
182 region targeted by *vqmR* from representative strains across sequenced vibrio species.
183
184 First, we discuss LuxT repression of P*vqmR*. Vibrio P*vqmR* sequence comparisons are
185 shown in a pair-wise sequence similarity color-map (Figure 4A, blue indicating highest
186 similarity). We compared a 50-nucleotide region from -48 to +2 relative to the *vqmR*
187 transcriptional start sites. This sequence space contains 20 nucleotides corresponding to
188 the LuxT$_{Vc}$ binding site (-28 to -9), together with 20 upstream and 10 downstream
189 nucleotides. We analyzed one representative genome across sixty-three different vibrios
190 that harbor both *luxT* and *vqmR*. For simplicity, only the LuxT consensus binding site is
191 shown in the figure, and it varies across P*vqmR* sequences. To test LuxT tolerance for
192 variation in binding site, we chose a few similar and quite different putative LuxT binding
193 sites from the set of *vqmR* promoters and performed EMSA analyses using 6X-His-
194 LuxT$_{Vc}$. The test sites come from P*vqmR* in *Vibrio metoecus*, *Vibrio splendidus*, and *V.*
195 *harveyi* (denoted P*vqmR*$_{Vm}$, P*vqmR*$_{Vs}$, and P*vqmR*$_{Vh}$, respectively, and are displayed in
196 Figure 4A). The *V. metoecus* P*vqmR* sequence is in the same cluster as the site bound
197 by LuxT$_{Vc}$ in P*vqmR*$_{Vc}$, differing by only 3 bp (sequence differences are highlighted in red
198 in Figure 4A). Not surprisingly, like P*vqmR*$_{Vc}$, LuxT$_{Vc}$ bound P*vqmR*$_{Vm}$ (Figure 4B). By
199 contrast, the LuxT binding sequences from *V. splendidus* and *V. harveyi*, which differ from
200 that in P*vqmR*$_{Vc}$ by ~40-50%, were not bound by LuxT$_{Vc}$ (Figure 4B). These findings
201 suggest that LuxT repression of P*vqmR* occurs only via DNA sequences present in *V.*
202 *cholerae* and closely related vibrios.

203

204 To further probe this hypothesis, we examined LuxT regulation of *vqmR* in *V. harveyi* by
205 qPCR. In this case, we predict that LuxT does not bind the *vqmR* promoter. As a positive
206 control for LuxT-dependent regulation, we measured expression of *swrZ*, a known *V.*
207 *harveyi* LuxT target (26). *vqmR* expression was the same in the *V. harveyi* parent and
208 Δ*luxT* strains (Supplementary Figure S7). By contrast, *swrZ* expression was ~100-fold
209 higher in the *V. harveyi* Δ*luxT* strain than the parent. Together, these results support the
210 conclusion that LuxT does not regulate *vqmR* in *V. harveyi*, consistent with the absence
211 of a LuxT binding site in the *V. harveyi vqmR* promoter.

212

213 Now we discuss VqmR repression of *luxT*. We have previously shown that the VqmR
214 sRNA binds to a 24 bp region encoding the first 8-amino acids of $LuxT_{Vc}$ (23). To
215 determine whether this N-terminal 8 amino acid extension is present in other vibrio LuxT
216 proteins, we compared this 24 bp region in *luxT* DNA sequences across vibrio genomes.
217 A pair-wise sequence similarity color-map shows that across vibrios, *luxT* genes separate
218 into multiple clusters. A majority cluster into a group that includes *V. harveyi*, and there is
219 a smaller cluster possessing *luxT* genes resembling that of *V. cholerae* (Figure 4C).
220 Notably, the *V. cholerae* start codon (TTG) in the *luxT* sequence is absent in vibrios that
221 are not closely related to *V. cholerae* (Figure 4C). Rather, in *V. harveyi* and its relatives,
222 *luxT* transcription is predicted to initiate at a downstream, ATG start codon. Consequently,
223 we predict that *V. harveyi* $LuxT_{Vh}$ and vibrios in the $LuxT_{Vh}$ cluster will produce a shorter
224 LuxT isoform that lacks the 8 N-terminal amino acids present in *V. cholerae* LuxT. These
225 findings imply that VqmR might only repress production of $LuxT_{Vc}$ but not LuxT in vibrios
226 that contain LuxT proteins that cluster with $LuxT_{Vh}$.

227

228 **The N-terminal 8 amino acids in *V. cholerae* LuxT expand the DNA motifs to which**
229 **LuxT can bind.** Our bioinformatic results suggest that the 24 bp region encoding the first
230 8 amino acids of $LuxT_{Vc}$ is specific to *V. cholerae*. We wondered whether having that N-
231 terminal amino acid extension is accompanied by functional consequences on the ability
232 of $LuxT_{Vc}$ to bind DNA. To explore this idea, we purified 6X-His-$LuxT_{Vc}$ and 6X-His-$LuxT_{Vc}$
233 $_{\Delta 8\text{-AA N-term}}$, which lacks the first 8 N-terminal amino acids, and tested binding to P*vqmR*$_{Vc}$.

234 As expected, the probe was bound by $LuxT_{Vc}$, however, $LuxT_{Vc\ \Delta 8\text{-}AA\ N\text{-}term}$ displayed
235 minimal binding (Figure 5A). These results show that the first 8 amino acids in $LuxT_{Vc}$ are
236 essential for binding to P*vqmR*$_{Vc}$. We also examined whether the absence of the first eight
237 amino acids in LuxT affected binding at other target DNA promoter sequences. As
238 mentioned, in *V. harveyi*, $LuxT_{Vh}$ regulates *swrZ* (P*swrZ*$_{Vh}$) encoding a GntR type
239 transcriptional regulator (26). As no LuxT-controlled genes other than *vqmR* were known
240 in *V. cholerae*, we assessed $LuxT_{Vc}$ binding to P*swrZ*$_{Vh}$ as a surrogate (see note on a *V.*
241 *cholerae* LuxT-controlled gene, *hapR*, reported during our ongoing work, in the
242 Discussion (27)). Both $LuxT_{Vc}$ and $LuxT_{Vc\ \Delta 8\text{-}AA\ N\text{-}term}$ bound with similar affinities to
243 P*swrZ*$_{Vh}$, demonstrating that while the first 8 amino acids of LuxT are necessary to bind
244 P*vqmR*$_{Vc}$, they are dispensable for binding to P*swrZ*$_{Vh}$ (Figure 5B). Below, we explore
245 $LuxT_{Vc}$ regulation of *V. cholerae* genes beyond *vqmR*.
246
247 To pinpoint the sequence in the -110 to +20 P*swrZ*$_{Vh}$ probe that is bound by $LuxT_{Vc}$, we
248 assayed seven overlapping DNA fragments spanning the region. Comparison of the
249 binding profiles suggested that multiple, non-continuous sequences are bound by $LuxT_{Vc}$
250 (Supplementary Figure S8). Consistent with this result, alignment of the P*swrZ* sequences
251 across vibrio species revealed two conserved sequence segments separated by 18 bp.
252 These sequences are ~15 bp in length, divergently oriented, and differ by four bp. The
253 first sequence is TAATCAGTACGCTGT (designated Motif 2L (for Left); -73 to -59), and
254 the second is AACTACGTACTGTTT (designated Motif 2R (for Right); -41 to -27) (Figure
255 5C, Supplementary Figures S9 and S10). Motif 2L and Motif 2R share a GTAC core with
256 the Motif 1 sequence, however their flanking regions differ. Notably, neither Motif 2L or
257 2R exist in P*vqmR*$_{Vc}$.
258
259 To test whether Motif 2L and Motif 2R support $LuxT_{Vc}$ binding, we assayed a probe
260 spanning P*swrZ*$_{Vh}$ -110 to +20 (containing both Motif 2L and Motif 2R) and compared it to
261 probes in which one or both motifs were scrambled. Probes containing at least one intact
262 motif supported $LuxT_{Vc}$ binding, while binding did not occur when both motifs were
263 scrambled (Figure 5D). Incubation of $LuxT_{Vc}$ with the P*swrZ*$_{Vh}$ probe containing both
264 motifs resulted in two band shifts, whereas probes containing only a single motif yielded

265 one band shift. These results suggest that LuxT can bind Motif 2L and Motif 2R individually
266 and simultaneously. Other TetR family proteins, such as QacR, also bind to motifs located
267 in close proximity (28). We also assessed binding of $LuxT_{Vh}$ to various versions of P*swrZ*$_{Vh}$
268 -110 to +20 fragments. The $LuxT_{Vh}$ binding profile was similar to that of $LuxT_{Vc}$
269 (Supplementary Figure S11).
270
271 To examine sufficiency of Motif 2L and Motif 2R for binding by LuxT, we used 15 bp probes
272 containing exclusively Motif 2L or Motif 2R. Both $LuxT_{Vc}$ and $LuxT_{Vh}$ bound to these
273 fragments, albeit with lower affinity than to the corresponding full-length probes. Thus, the
274 Motif 2L and Motif 2R DNA sequences are sufficient for LuxT binding, and the flanking
275 residues promote stronger binding (Supplementary Figure S12).
276
277 We conclude that $LuxT_{Vc}$ can recognize Motif 1, Motif 2L, and Motif 2R. Moreover, the N-
278 terminal 8 amino acids in $LuxT_{Vc}$ are dispensable for $LuxT_{Vc}$ to bind P*swrZ*$_{Vh}$. Given that
279 these N-terminal 8 amino acids are required for $LuxT_{Vc}$ to bind Motif 1 in P*vqmR*$_{Vc}$, we
280 infer that harboring these amino acids expands the possibilities for *V. cholerae* LuxT to
281 control gene expression.
282
283 **$LuxT_{Vc}$ promotes biofilm formation in *V. cholerae* at low cell density.** A previous RNA-
284 Seq study in *V. harveyi* identified that the $LuxT_{Vh}$ regulon includes *swrZ* and ~10 genes
285 specifying GGDEF or EAL domain-containing proteins that synthesize and degrade,
286 respectively, the second messenger c-di-GMP molecule (26). In *V. cholerae,* c-di-GMP
287 levels influence biofilm formation (29, 30). Thus, we wondered whether $LuxT_{Vc}$ regulates
288 biofilm formation. To assess this possibility, we monitored colony biofilm morphologies of
289 the *V. cholerae* Δ*tdh* and Δ*tdh* Δ*luxT* strains. In *V. cholerae*, biofilm formation drives a
290 change in colony appearance from smooth to wrinkled, with the latter coinciding with an
291 increase in colony height (31–34). Thus, three-dimensional colony height profiles track
292 with biofilm formation. Figure 6 shows images of biofilm colonies and their corresponding
293 height profiles, quantitation of which are displayed as heatmaps. Both the Δ*tdh* and Δ*tdh*
294 Δ*luxT* strains failed to form biofilms.
295

296 The master high cell density QS regulator HapR is a key repressor of *V. cholerae* biofilm
297 formation (11, 29). Thus, we reasoned that $LuxT_{Vc}$-dependent biofilm phenotypes might
298 be revealed in the absence of *hapR*. Indeed, Figure 6 shows that while the Δ*tdh* Δ*hapR*
299 strain formed colony biofilms with heights reaching up to ~550 µm, heights of Δ*tdh* Δ*hapR*
300 Δ*luxT* colonies reached only ~250 µm. As expected, complementation of the Δ*hapR*
301 Δ*luxT* strain with *luxT* on a plasmid restored biofilm formation (Supplementary Figure
302 S13) Thus, *V. cholerae* forms colony biofilms only in the absence of HapR and, in this low
303 cell density context, $LuxT_{Vc}$ promotes biofilm formation.
304
305 Production of the VqmR sRNA at high cell density suppresses colony biofilm formation
306 (18, 23). To probe whether $LuxT_{Vc}$ modulates biofilm formation via control of *vqmR*, we
307 compared colony morphologies of the Δ*tdh* Δ*hapR* Δ*vqmA* and Δ*tdh* Δ*hapR* Δ*vqmA* Δ*luxT*
308 strains. VqmA is required for activation of $P_{vqmR_{Vc}}$, thus in its absence, *vqmR* is not
309 expressed (23). The Δ*tdh* Δ*hapR* Δ*vqmA* strain formed colony biofilms similar to those of
310 the Δ*tdh* Δ*hapR* strain with heights reaching up to ~550 µm, while colony biofilms of the
311 Δ*tdh* Δ*hapR* Δ*vqmA* Δ*luxT* strain had heights of ~250 µm (Figure 6). Thus, $LuxT_{Vc}$
312 activates biofilm formation. Moreover, in our assays, endogenous levels of VqmA and
313 VqmR do not influence colony biofilm formation so $LuxT_{Vc}$ must drive biofilm formation by
314 a mechanism that is independent of VqmA and VqmR.
315
316 **$LuxT_{Vc}$ controls a regulon of *V. cholerae* genes at high cell density.** Given that $LuxT_{Vc}$
317 binds to distinct DNA motifs and it regulates *V. cholerae* biofilm formation independently
318 of VqmA-VqmR, we reasoned that $LuxT_{Vc}$ may control additional genes. To define the *V.*
319 *cholerae* $LuxT_{Vc}$-controlled regulon, we conducted RNA-Seq on the *V. cholerae* Δ*tdh*
320 Δ*luxT* strain carrying plasmid-borne $luxT_{Vc}$ under control of the arabinose promoter (p-
321 P_{BAD}-$luxT_{Vc}$). Following growth to high cell density in the presence and absence of
322 arabinose, approximately 20 genes displayed changes in expression of >2-fold (Figure
323 7). As anticipated, $luxT_{Vc}$ was the most upregulated gene in the dataset. Other $LuxT_{Vc}$-
324 regulated genes included ones involved in galactose and sulfate metabolism, which were
325 activated and repressed ~2-4 fold, respectively. Alteration of expression of a gene
326 specifying an orphan histidine kinase (*vc1088*, ~3-fold) occurred. *vc1088* resides

327 immediately adjacent to an 8-gene operon (*vc1080-vc1087*) encoding genes involved in
328 nitric oxide sensing and biofilm formation (35–37). Additionally, several genes specifying
329 hypothetical proteins or those with domains of unknown function were differentially
330 expressed. Other than *vc1088*, which, given its genomic context, we hypothesize is a
331 regulator of biofilm genes, the regulon did not harbor genes known to be involved in
332 biofilm formation. This result was expected because the strain used in the RNA-Seq
333 experiment possesses HapR, and as shown in Figure 6, HapR represses biofilm
334 formation at high cell density. Also, as expected, we did not identify *vqmR* because our
335 sample preparation was not optimized for enrichment of sRNAs. The RNA-Seq data,
336 together with the other findings from the above studies, suggest that LuxT acts broadly to
337 regulate signaling and metabolic pathways in *V. cholerae*, ranging from QS to biofilm
338 formation to sulfate metabolism.
339
340 **Discussion**
341 Here, we used a genetic screen to identify repressors of the *V. cholerae* DPO-VqmA-
342 VqmR QS circuit. Our screen revealed four genes: *acy*, *crp*, *wigR*, and *luxT*. We first
343 interpret our findings regarding *acy*, *crp*, *wigR* in the context of QS regulation and then
344 we discuss *luxT*, the gene we focused on in the current study.
345
346 The *acy* and *crp* genes encode adenylate cyclase (Acy) and the cAMP receptor protein
347 (Crp), respectively. Acy and Crp typically function together (38–40). Acy synthesizes
348 cAMP, which is bound by Crp. The Crp-cAMP complex regulates transcription of target
349 genes, particularly those involved in utilization of different carbon sources. Given this well-
350 established partnership, it is surprising that we find that Acy and Crp apparently work
351 independently of each other to control the DPO-VqmA-VqmR QS circuit with Acy affecting
352 VqmA activity, and Crp modifying P*vqmR* expression. *V. cholerae* possesses at least two
353 additional Crp family proteins, neither of which have been studied. One or both of them
354 could partner with Acy to regulate VqmA activity. WigR is a response regulator that, with
355 its partner kinase WigK, constitutes a two-component system that is proposed to monitor
356 cell wall damage (41, 42). Our finding suggests the possibility that cell wall damage feeds
357 into QS control of gene expression.

358

359 LuxT is a TetR-family transcriptional regulator. TetR-family proteins frequently bind small-
360 molecule ligands and a target DNA motif (43). We demonstrate that *V. cholerae* LuxT
361 binds DNA; it remains to be determined whether it binds a ligand. *luxT* is conserved
362 across vibrio species. In *V. harveyi*, LuxT represses expression of the gene encoding the
363 QS sRNA called Qrr1 at low cell density, a function conserved in several vibrio species
364 but not in *V. cholerae* (25). By contrast, we show that in *V. cholerae*, LuxT represses
365 expression of the gene encoding the VqmR sRNA, and this feature is not conserved in *V.*
366 *harveyi.* Thus, as a broader regulatory theme, LuxT represses genes encoding sRNAs
367 that function at the hearts of QS systems. In the context of LuxT regulation of QS
368 components, we note that, after we concluded our experiments, a study was published
369 reporting that $LuxT_{Vc}$ binds P$hapR_{Vc}$. The motif identified is similar to that in P$vqmR_{Vc}$
370 (Figure 5D) (27).
371

372 Our findings also reveal that VqmR post-transcriptionally represses LuxT by targeting the
373 mRNA region encoding its first eight amino acids. The eight N-terminal amino acid
374 residues are required for LuxT to bind the *vqmR* promoter. Furthermore, while $LuxT_{Vc\ \Delta 8\text{-}AA\ N\text{-}term}$
375 fails to bind the *vqmR* promoter, it nonetheless retains binding to another
376 promoter, P*swrZ*. LuxT in other vibrios lacks this N-terminal extension. We propose that
377 the acquisition of the LuxT N-terminal 8 amino acids delivers three activities: it allows
378 repression of *luxT* by VqmR, it enables LuxT binding to the *vqmR* promoter to establish
379 the VqmR-LuxT double-negative feedback loop, and it promotes regulon expansion by
380 broadening the DNA motifs to which LuxT can bind (Figure 1). To our knowledge, this is
381 the first example in which the mRNA sequence that is targeted by a sRNA regulator
382 encodes a portion of a protein that governs that protein's DNA-binding capabilities.
383

384 Double negative feedback loops are common in biological systems requiring tight
385 regulation of state transitions. For instance, in bacteriophage λ, the cI and Cro proteins
386 mutually repress each other to control the switch between lysogenic and lytic cycles (44).
387 Similarly, in *Sinorhizobium meliloti*, a double negative feedback loop between the NtrBC
388 two-component system and the sRNA NfeR1 modulates nitrogen metabolism (45). In *V.*

389 *cholerae*, the transition from low cell density to high cell density QS modes involves
390 upregulation of genes encoding energetically costly processes such as motility and the
391 type six secretion system (7, 46, 47). Thus, the double negative feedback between LuxT
392 and VqmR may serve as a buffer that prevents inappropriate transitions between states
393 until conditions are optimal.
394
395 In *V. cholerae*, we find that LuxT promotes biofilm formation in a strain genetically locked
396 into expressing low cell density QS behaviors. The mechanism by which LuxT mediates
397 this effect remains undefined but is independent of HapR. Preliminary analyses of
398 promoter regions of canonical biofilm genes do not reveal recognizable LuxT binding
399 motifs, raising the possibility that LuxT binds to an uncharacterized DNA sequence in
400 these promoters or, alternatively, it indirectly regulates biofilm formation genes. That LuxT
401 regulates biofilm formation is particularly intriguing in light of recent work in *V. harveyi*,
402 where LuxT was shown to be a global regulator of gene expression at low cell density
403 (25, 26). Here, we primarily characterized LuxT functions in *V. cholerae* at high cell
404 density. Studies to identify the full *V. cholerae* LuxT regulon across different cell densities
405 are required to delineate the scope of its regulatory roles.
406
407 Biofilm formation is required for *V. cholerae* to colonize the anaerobic intestinal lumen of
408 infant mice and to form communities on human host cells (27, 48–50). Given that *luxT*
409 and the DPO-VqmA-VqmR QS circuit are responsive to oxygen levels and human-host
410 produced bile salts, future studies could examine the roles of LuxT, the DPO-VqmA-VqmR
411 QS circuit, and the VqmR-LuxT double negative feedback during the *V. cholerae*
412 infectious lifecycle (24, 27).
413
414 The regulatory logic uncovered here highlights how a modest genetic innovation, the eight
415 amino acid N-terminal extension in *V. cholerae* LuxT, generates a pathogen-specific
416 signaling architecture that links sRNA-mediated post-transcriptional control to
417 transcription factor DNA-binding specificity. This dual-function sequence represents, to
418 our knowledge, the first example in which a sRNA binding site also encodes a domain
419 required for the encoded protein's regulatory activity. Moreover, the LuxT-VqmR feedback

420 loop is restricted to *V. cholerae* and its close relatives, illustrating how QS circuits can be
421 rewired to produce species-specific behaviors. These findings provide conceptual insight
422 into evolution of new regulatory modules and help us understand how QS networks can
423 be tailored to particular ecological niches.
424
425 **Materials and Methods:**
426 **Bacterial growth, strain construction and reagents.** *Escherichia coli* Top10 and
427 *Saccharomyces cerevisiae* were used as hosts for cloning, while *E. coli* S17-1 λ*pir* was
428 used for conjugations. Cultures of *V. cholerae* and *E. coli* were grown in LB medium at
429 37°C with shaking. When required, media were supplemented with streptomycin, 200
430 µg/mL; kanamycin, 50 µg/mL; polymyxin B, 50 µg/mL; chloramphenicol, 1 µg/mL;
431 spectinomycin, 200 µg/mL. Bioluminescence-reporter assays were conducted as
432 previously described (24). Where indicated, relative light units (RLU) denote
433 bioluminescence output divided by the culture optical density.
434
435 Chromosomal alterations were introduced into *V. cholerae* using multiplexed genome
436 editing (MuGENT) or the pRE112 suicide vector harboring the counter-selectable *sacB*
437 gene as previously described (24, 51). Unless otherwise specified, chromosomal DNA
438 from *V. cholerae* C6706 was used as the template for PCR reactions. Plasmids were
439 constructed using pBAD-pEVS or pRE112 as backbones and assembled using NEB Hi-
440 Fi reagent or yeast-recombination-assisted assembly as previously described (52).
441 Strains, plasmids, and oligonucleotides used in the study are listed in Supplementary
442 Tables 1, 2, and 3, respectively.
443
444 Gel purification and plasmid preparation kits, iProof DNA polymerase, and
445 Deoxynucleotide Mix were purchased from Qiagen, Bio-Rad, and New England Biolabs,
446 respectively.
447
448 **Sequence analyses.** Sequence-similarity based identification of *luxT* and *vqmR* genes
449 across vibrio genomes has been described (25, 53). A custom MATLAB (MathWorks;
450 2022) algorithm was used to search for *luxT* and *vqmR* genes in the genomes of 134

451 vibrio strains, each representing a distinct species. The initial search identified 63 vibrio
452 species harboring both *luxT* and *vqmR* genes. We further analyzed these species for
453 sequence conservation within each gene as well as their promoters. Multiple sequence
454 alignments were performed and the output analyzed in MATLAB. A standard scoring
455 matrix NUC44 (see ftp.ncbi.nih.gov/blast/matrices/) was used to compute similarity
456 scores between DNA sequences. The unweighted pair group method with arithmetic
457 mean (UPGMA) was subsequently used to cluster vibrio species with similar sequences.
458
459 **Protein purification.** Genes encoding 6X-His-tagged proteins were cloned into pET15b
460 and transformed into *E. coli* BL21. Strains for protein production were cultured in LB with
461 100 µg/mL ampicillin and incubated at 37°C with aeration. When cultures reached an
462 OD_{600} of 0.5, 400 µM IPTG was added to induce protein production. The cultures were
463 further incubated at 18°C overnight. Cells were harvested via centrifugation at 4,000 rpm
464 for 10 min. The resulting cell pellets were resuspended in 1/100 volume of lysis buffer (50
465 mM Tris-HCl, 150 mM NaCl, pH 8) containing 5 µM benzonase, 3 µM imidazole, 250
466 µg/mL lysozyme, and BugBuster Protein Extraction Reagent (Novagen). The lysate was
467 subjected to centrifugation at 13,000 rpm for 20 min, and the clarified supernatant was
468 combined with Ni-NTA Superflow resin (Qiagen) equilibrated with 3 µM imidazole. After
469 allowing the resin and protein to incubate for 1 h at 4°C, the resin was subjected to a
470 series of washes with imidazole at concentrations from 3 µM to 40 µM. Protein was eluted
471 from the resin with buffer (50 mM Tris-HCl, 150 mM NaCl, pH 8) containing 300 µM
472 imidazole. Purified protein was dialyzed overnight at 4°C with Slide-A-Lyzer modules
473 (Thermo Fisher) in buffer (50 mM Tris-HCl, 150 mM NaCl, pH 8), concentrated, flash-
474 frozen, and stored at -80°C.
475
476 **Bioluminescence measurements.** Strains harboring luciferase reporters were cultured
477 overnight at 37°C in LB and diluted into fresh LB at a final OD_{600} = 0.0025. Where
478 indicated, the medium was supplemented with 640 nM DPO. 150 µL of the cultures were
479 transferred to 96-well plates with transparent bottoms. Where indicated expression of the
480 pBAD promoter was induced with 0.007% to 0.2% arabinose. Plates were incubated at
481 37°C. Bioluminescence production and OD_{600} were measured using a BioTek Synergy

482 Neo2 HTS multimode microplate reader. Reporter activity is presented as Relative Light
483 Units (RLUs), which is bioluminescence divided by OD_{600}.
484
485 **Transposon mutagenesis screen and identification of insertion sites.** Mutagenesis
486 was performed as previously described using a Tn*5* transposon system carrying
487 kanamycin resistance (54). Transposons were introduced into the Δ*tdh vqmA*$_{C134A\text{-}FLAG}$
488 P*vqmR-lux V. cholerae* strain by conjugation from an *E. coli* donor. Conjugation was
489 limited to 2 h to reduce the likelihood of recovering sibling insertion events. Exconjugants
490 were selected on LB agar supplemented with kanamycin, polymyxin B, and X-gal (54).
491 Following overnight growth at 37°C, colonies were examined for changes in color.
492 Mutants displaying increased blue color relative to the plate average were purified by
493 restreak on LB agar containing kanamycin and polymyxin B. Transposon insertion sites
494 were mapped using arbitrary PCR, as described previously (54).
495
496 **Electromobility gel shift assays (EMSAs).** DNA probes were purchased as G-Blocks
497 from IDT (~200 bp) and were used as templates for PCR amplification. The resulting PCR
498 products were gel purified using the QIAquick Gel Purification kit (Qiagen), eluted with
499 sterile water, and stored at 4°C until use. Alternatively, duplex DNA oligomers (~20-30 bp)
500 were purchased from IDT and used in assays. To initiate EMSA assays, 0.6 to 6 μM of
501 purified protein in buffer (50 mM Tris-HCl, 150 mM NaCl, pH 8) was combined with DNA
502 probes normalized to 5-15 ng. Mixtures were reacted for 20 min at room temperature and
503 subsequently subjected to electrophoresis on Novex 6% DNA Retardation Gels (Thermo
504 Fisher) in 1X Tris-buffered EDTA (TBE) at 4°C (24). DNA probes were visualized with
505 Sybr Green stain (Thermo Fisher) and imaged with an ImageQuant 800 imaging system
506 (Cytiva) (24).
507
508 **Immunoblotting**. *V. cholerae* strains were cultured overnight in M9 minimal medium. The
509 next day, the cultures were diluted 1:1000 into fresh M9 medium containing 0.01%
510 arabinose and grown to an OD_{600} of 1. Cells were pelleted by centrifugation and
511 resuspended in 20 μL of ice-cold phosphate-buffered saline (PBS) at an OD_{600} of 3.5.
512 Cells were lysed, protein extracts were separated on SDS-PAGE gels, and

513 immunoblotting was performed as described previously (24). Protein levels were
514 assessed using ImageJ software.
515
516 **Biofilm assays and image analyses.** *V. cholerae* strains were cultured overnight in LB
517 medium at 37°C with aeration. Cultures were subjected to vortex for 5 min with 4 mm
518 glass beads added to disrupt cell aggregates. The samples were diluted to OD_{600} = 0.5 in
519 1X PBS. The cultures were again subjected to vortex for 5 min without beads. 1 µL of
520 each culture was spotted onto an LB plate containing 50 mg/mL polymyxin B. When
521 strains carried plasmids, plates contained 40 mg/mL polymyxin B, 25 mg/mL kanamycin,
522 and, when specified, 0.01% arabinose. The plates were incubated at 37°C and biofilms
523 were imaged every 24 h with a Leica M125 stereomicroscope. Colony height profiles were
524 captured using a Keyence VK-X3000 laser microscope (31). Images were analyzed using
525 the manufacturer provided MultiFileAnalyzer application. Lateral topographic cross
526 sections were profiled in triplicate. For each cross section, the program identified the
527 minimum and maximum heights.
528
529 **qPCR**. Overnight cultures of *V. harveyi* were diluted to OD_{600} = 0.0025 and grown to OD_{600}
530 = 0.1 in LM medium. The cultures were treated with RNAprotect (Qiagen) and RNA was
531 purified using the RNeasy Mini Kit (Qiagen). gDNA was degraded and cDNA was
532 generated using SuperScript IV VILO Master Mix with ezDNAse (ThermoFisher) using
533 the manufacturer's recommended procedures. RNA was quantified using PerfeCTa
534 SYBR Green FastMix with Low ROX (QuantaBio). Relative RNA quantities were
535 calculated by $\Delta\Delta Ct$ compared to WT and the reference gene, *hfq*.
536
537 **RNA sequencing**. Overnight cultures of *V. cholerae* were diluted to OD_{600} = 0.0025 and
538 grown to OD_{600} = 0.05 in LB. Cultures were divided in half: 0.1% arabinose was
539 administered to one half and the other half received LB as a control. The treated cultures
540 were grown to OD_{600} = 0.25. RNA Protect solution (Qiagen) was added at 2:1 v/v
541 reagent:culture and RNA was purified using the RNeasy Mini Kit (Qiagen) followed by
542 treatment with DNase (Ambion AM 1907) using the manufacturers' recommended

procedures with minor modifications are described previously (7). RNA samples were sequenced by SeqCenter (Pittsburgh, PA).

Acknowledgments

We thank Bassler group members for thoughtful discussions. This work was supported by the Howard Hughes Medical Institute and NSF grant MCB-2508324 to B.L.B. A.A.M. was supported as a Howard Hughes Medical Institute Fellow of the Life Sciences Research Foundation and, subsequently, as a member of the Stowers Institute for Medical Research.

Author contributions

A.A.M., K.D., J.V., C.F., and B.L.B. designed experiments and analyzed data; A.A.M., K.D., and J.V. constructed strains and performed wet-lab experiments; C.F., A.A.M., and B.L.B. designed bioinformatic experiments and C.F. performed bioinformatic experiments and analyses; K.D., C.F., and A.A.M., wrote custom scripts for data analyses and visualization; A.A.M., K.D., and B.L.B. wrote the original draft; A.A.M., K.D., J.V., C.F., and B.L.B. reviewed and edited subsequent manuscript versions; B.L.B. provided oversight, resources, and funding.

References:

1. Bassler BL. 1999. How bacteria talk to each other: regulation of gene expression by quorum sensing. Current Opinion in Microbiology 2:582–587.
2. Schauder S, Bassler BL. 2001. The languages of bacteria. Genes Dev 15:1468–1480.
3. Papenfort K, Bassler BL. 2016. Quorum sensing signal–response systems in Gram-negative bacteria. Nat Rev Microbiol 14:576–588.
4. Svenningsen SL, Waters CM, Bassler BL. 2008. A negative feedback loop involving small RNAs accelerates Vibrio cholerae's transition out of quorum-sensing mode. Genes Dev 22:226–238.
5. van Kessel JC, Rutherford ST, Shao Y, Utria AF, Bassler BL. 2013. Individual and Combined Roles of the Master Regulators AphA and LuxR in Control of the *Vibrio harveyi* Quorum-Sensing Regulon. J Bacteriol 195:436–443.
6. Rutherford ST, van Kessel JC, Shao Y, Bassler BL. 2011. AphA and LuxR/HapR reciprocally control quorum sensing in vibrios. Genes Dev 25:397–408.
7. Mashruwala AA, Qin B, Bassler BL. 2022. Quorum-sensing- and type VI secretion-mediated spatiotemporal cell death drives genetic diversity in *Vibrio cholerae*. Cell 185:3966-3979.e13.
8. Shao Y, Bassler BL. 2014. Quorum regulatory small RNAs repress type VI secretion in *Vibrio cholerae*. Mol Microbiol 92:921–930.
9. Suckow G, Seitz P, Blokesch M. 2011. Quorum Sensing Contributes to Natural Transformation of *Vibrio cholerae* in a Species-Specific Manner ▿ . J Bacteriol 193:4914–4924.
10. Tsou AM, Frey EM, Hsiao A, Liu Z, Zhu J. 2008. Coordinated regulation of virulence by quorum sensing and motility pathways during the initial stages of *Vibrio cholerae* infection. Commun Integr Biol 1:42–44.
11. Hammer BK, Bassler BL. 2003. Quorum sensing controls biofilm formation in *Vibrio cholerae* : Biofilms in *Vibrio cholerae*. Molecular Microbiology 50:101–104.
12. Zhu J, Mekalanos JJ. 2003. Quorum Sensing-Dependent Biofilms Enhance Colonization in *Vibrio cholerae*. Developmental Cell 5:647–656.
13. Zhu J, Miller MB, Vance RE, Dziejman M, Bassler BL, Mekalanos JJ. 2002. Quorum-sensing regulators control virulence gene expression in *Vibrio cholerae*. Proc Natl Acad Sci USA 99:3129–3134.
14. Higgins DA, Pomianek ME, Kraml CM, Taylor RK, Semmelhack MF, Bassler BL. 2007. The major *Vibrio cholerae* autoinducer and its role in virulence factor production. Nature 450:883–886.
15. Bridges AA, Fei C, Bassler BL. 2020. Identification of signaling pathways, matrix-digestion enzymes, and motility components controlling *Vibrio cholerae* biofilm dispersal. Proc Natl Acad Sci U S A 117:32639–32647.
16. Bridges AA, Bassler BL. 2019. The intragenus and interspecies quorum-sensing autoinducers exert distinct control over *Vibrio cholerae* biofilm formation and dispersal. PLoS Biol 17:e3000429.
17. Miller MB, Skorupski K, Lenz DH, Taylor RK, Bassler BL. 2002. Parallel Quorum Sensing Systems Converge to Regulate Virulence in *Vibrio cholerae*. Cell 110:303–314.
18. Papenfort K, Silpe JE, Schramma KR, Cong J-P, Seyedsayamdost MR, Bassler BL. 2017. A *Vibrio cholerae* autoinducer–receptor pair that controls biofilm formation. Nat Chem Biol 13:551–557.

19. Chen X, Schauder S, Potier N, Van Dorsselaer A, Pelczer I, Bassler BL, Hughson FM. 2002. Structural identification of a bacterial quorum-sensing signal containing boron. Nature 415:545–549.
20. Jung SA, Chapman CA, Ng W-L. 2015. Quadruple Quorum-Sensing Inputs Control *Vibrio cholerae* Virulence and Maintain System Robustness. PLoS Pathog 11:e1004837.
21. Barrasso K, Watve S, Simpson CA, Geyman LJ, van Kessel JC, Ng W-L. 2020. Dual-function quorum-sensing systems in bacterial pathogens and symbionts. PLoS Pathog 16:e1008934.
22. Lacey DM, D'Agostino GD, Shine EE, Bassler BL. 2026. Multiple Adenylate-Forming Enzymes Contribute to Biosynthesis of the DPO Quorum-Sensing Autoinducer. ACS Chem Biol 21:380–391.
23. Papenfort K, Förstner KU, Cong J-P, Sharma CM, Bassler BL. 2015. Differential RNA-seq of *Vibrio cholerae* identifies the VqmR small RNA as a regulator of biofilm formation. Proc Natl Acad Sci USA 112.
24. Mashruwala AA, Bassler BL. 2020. The *Vibrio cholerae* Quorum-Sensing Protein VqmA Integrates Cell Density, Environmental, and Host-Derived Cues into the Control of Virulence 11.
25. Eickhoff MJ, Fei C, Huang X, Bassler BL. 2021. LuxT controls specific quorum-sensing-regulated behaviors in Vibrionaceae spp. via repression of qrr1, encoding a small regulatory RNA. PLoS Genet 17:e1009336.
26. Eickhoff MJ, Fei C, Cong J-P, Bassler BL. 2022. LuxT Is a Global Regulator of Low-Cell-Density Behaviors, Including Type III Secretion, Siderophore Production, and Aerolysin Production, in *Vibrio harveyi* 13.
27. Li Y, Yan J, Li J, Xue X, Wang Y, Cao B. 2023. A novel quorum sensing regulator LuxT contributes to the virulence of *Vibrio cholerae*. Virulence 14:2274640.
28. Schumacher MA, Miller MC, Grkovic S, Brown MH, Skurray RA, Brennan RG. 2002. Structural basis for cooperative DNA binding by two dimers of the multidrug-binding protein QacR. EMBO J 21:1210–1218.
29. Waters CM, Lu W, Rabinowitz JD, Bassler BL. 2008. Quorum Sensing Controls Biofilm Formation in *Vibrio cholerae* through Modulation of Cyclic Di-GMP Levels and Repression of *vpsT*. J Bacteriol 190:2527–2536.
30. Krasteva PV, Fong JCN, Shikuma NJ, Beyhan S, Navarro MVAS, Yildiz FH, Sondermann H. 2010. *Vibrio cholerae* VpsT Regulates Matrix Production and Motility by Directly Sensing Cyclic di-GMP. Science 327:866–868.
31. Yan J, Fei C, Mao S, Moreau A, Wingreen NS, Košmrlj A, Stone HA, Bassler BL. 2019. Mechanical instability and interfacial energy drive biofilm morphogenesis. eLife 8:e43920.
32. Casper-Lindley C, Yildiz FH. 2004. VpsT is a transcriptional regulator required for expression of vps biosynthesis genes and the development of rugose colonial morphology in *Vibrio cholerae* O1 El Tor. J Bacteriol 186:1574–1578.
33. Fong JCN, Karplus K, Schoolnik GK, Yildiz FH. 2006. Identification and characterization of RbmA, a novel protein required for the development of rugose colony morphology and biofilm structure in *Vibrio cholerae*. J Bacteriol 188:1049–1059.
34. Fong JCN, Yildiz FH. 2007. The *rbmBCDEF* gene cluster modulates development of rugose colony morphology and biofilm formation in *Vibrio cholerae*. J Bacteriol 189:2319–2330.

35. Plate L, Marletta MA. 2012. Nitric oxide modulates bacterial biofilm formation through a multi-component cyclic-di-GMP signaling network. Mol Cell 46:449–460.
36. Anantharaman S, Guercio D, Mendoza AG, Withorn JM, Boon EM. 2023. Negative regulation of biofilm formation by Nitric Oxide Sensing Proteins. Biochem Soc Trans 51:1447–1458.
37. Hossain S, Heckler I, Boon EM. 2018. Discovery of a Nitric Oxide Responsive Quorum Sensing Circuit in *Vibrio cholerae*. ACS Chem Biol 13:1964–1969.
38. Liang W, Pascual-Montano A, Silva AJ, Benitez JA. 2007. The cyclic AMP receptor protein modulates quorum sensing, motility and multiple genes that affect intestinal colonization in *Vibrio cholerae*. Microbiology 153:2964–2975.
39. Liang W, Sultan SZ, Silva AJ, Benitez JA. 2008. Cyclic AMP post-transcriptionally regulates the biosynthesis of a major bacterial autoinducer to modulate the cell density required to activate quorum sensing. FEBS Letters 582:3744–3750.
40. Manneh-Roussel J, Haycocks JRJ, Magán A, Perez-Soto N, Voelz K, Camilli A, Krachler A-M, Grainger DC. 2018. cAMP Receptor Protein Controls Vibrio cholerae Gene Expression in Response to Host Colonization. mBio 9:e00966-18.
41. Dörr T, Alvarez L, Delgado F, Davis BM, Cava F, Waldor MK. 2016. A cell wall damage response mediated by a sensor kinase/response regulator pair enables beta-lactam tolerance. Proc Natl Acad Sci USA 113:404–409.
42. Cheng AT, Ottemann KM, Yildiz FH. 2015. *Vibrio cholerae* Response Regulator VxrB Controls Colonization and Regulates the Type VI Secretion System. PLoS Pathog 11:e1004933.
43. Cuthbertson L, Nodwell JR. 2013. The TetR Family of Regulators. Microbiol Mol Biol Rev 77:440–475.
44. Lee S, Lewis DEA, Adhya S. 2018. The Developmental Switch in Bacteriophage λ: A Critical Role of the Cro Protein. J Mol Biol 430:58–68.
45. García-Tomsig NI, García-Rodriguez FM, Guedes-García SK, Millán V, Becker A, Robledo M, Jiménez-Zurdo JI. 2023. A double-negative feedback loop between NtrBC and a small RNA rewires nitrogen metabolism in legume symbionts. mBio 14:e0200323.
46. Herzog R, Peschek N, Fröhlich KS, Schumacher K, Papenfort K. 2019. Three autoinducer molecules act in concert to control virulence gene expression in *Vibrio cholerae*. Nucleic Acids Research 47:3171–3183.
47. Mashruwala AA, Bassler BL. 2024. Quorum sensing orchestrates parallel cell death pathways in *Vibrio cholerae* via Type 6 secretion-dependent and -independent mechanisms. Proc Natl Acad Sci U S A 121:e2412642121.
48. Vidakovic L, Mikhaleva S, Jeckel H, Nisnevich V, Strenger K, Neuhaus K, Raveendran K, Ben-Moshe NB, Aznaourova M, Nosho K, Drescher A, Schmeck B, Schulte LN, Persat A, Avraham R, Drescher K. 2023. Biofilm formation on human immune cells is a multicellular predation strategy of *Vibrio cholerae*. Cell 186:2690-2704.e20.
49. Gallego-Hernandez AL, DePas WH, Park JH, Teschler JK, Hartmann R, Jeckel H, Drescher K, Beyhan S, Newman DK, Yildiz FH. 2020. Upregulation of virulence genes promotes *Vibrio cholerae* biofilm hyperinfectivity. Proceedings of the National Academy of Sciences 117:11010–11017.
50. Conner JG, Teschler JK, Jones CJ, Yildiz FH. 2016. Staying Alive: *Vibrio cholerae* 's Cycle of Environmental Survival, Transmission, and Dissemination. Microbiol Spectr 4:4.2.02.

51. Dalia AB, McDonough E, Camilli A. 2014. Multiplex genome editing by natural transformation. Proc Natl Acad Sci USA 111:8937–8942.
52. Joska TM, Mashruwala A, Boyd JM, Belden WJ. 2014. A universal cloning method based on yeast homologous recombination that is simple, efficient, and versatile. Journal of Microbiological Methods 100:46–51.
53. Duddy OP, Silpe JE, Fei C, Bassler BL. 2023. Natural silencing of quorum-sensing activity protects *Vibrio parahaemolyticus* from lysis by an autoinducer-detecting phage. PLOS Genetics 19:e1010809.
54. Jemielita M, Wingreen NS, Bassler BL. 2018. Quorum sensing controls *Vibrio cholerae* multicellular aggregate formation. Elife 7:e42057.

Figures and Figure Legends:

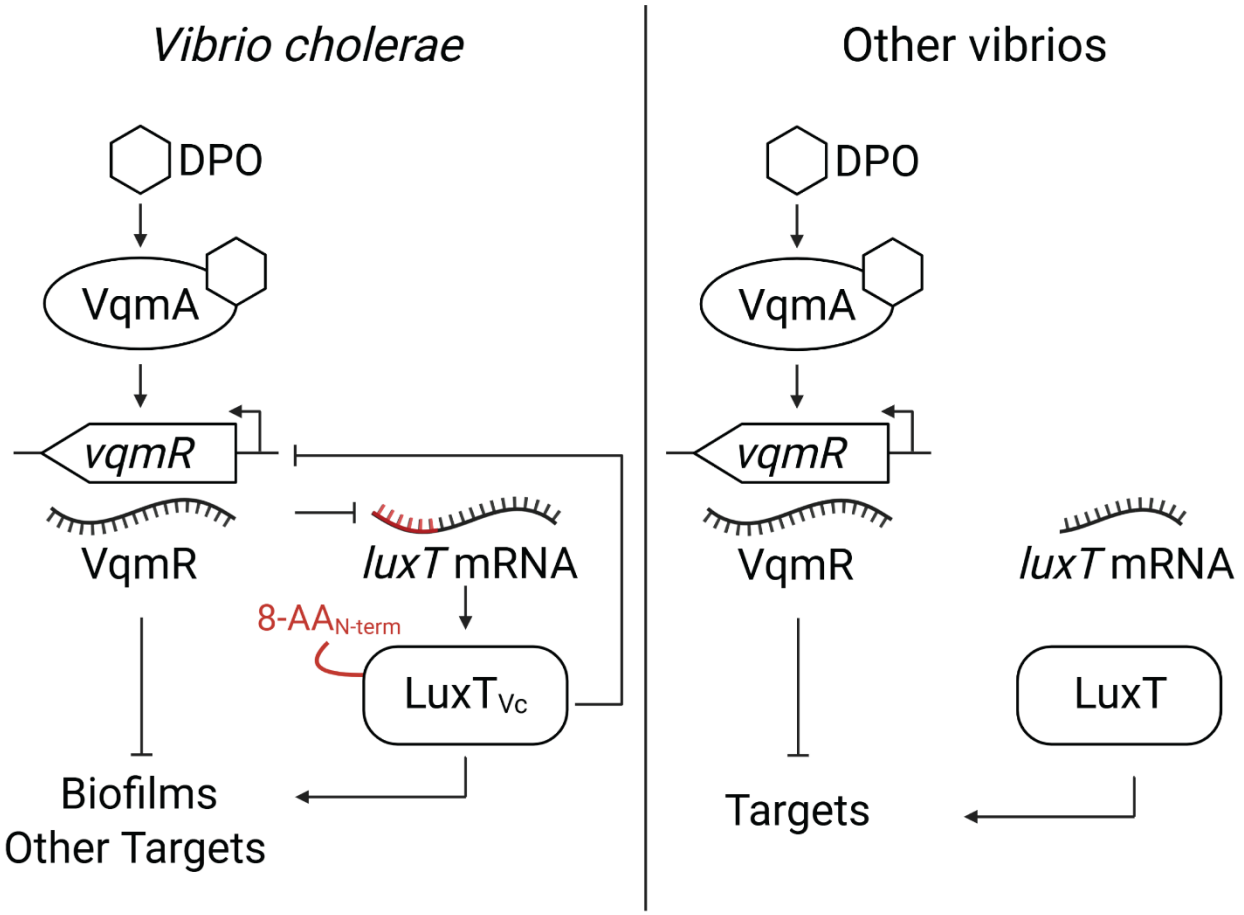

Figure 1. Simplified scheme for a double negative feedback loop comprised of the VqmR sRNA and the LuxT transcription factor. This regulatory loop exists in *V. cholerae* and closely related vibrios but not in more distant relatives. In the left panel, the designation 8-$AA_{N\text{-}term}$ on the LuxT protein and the red portion of the *luxT* mRNA show the regions required for the double negative feedback loop. See text for details.

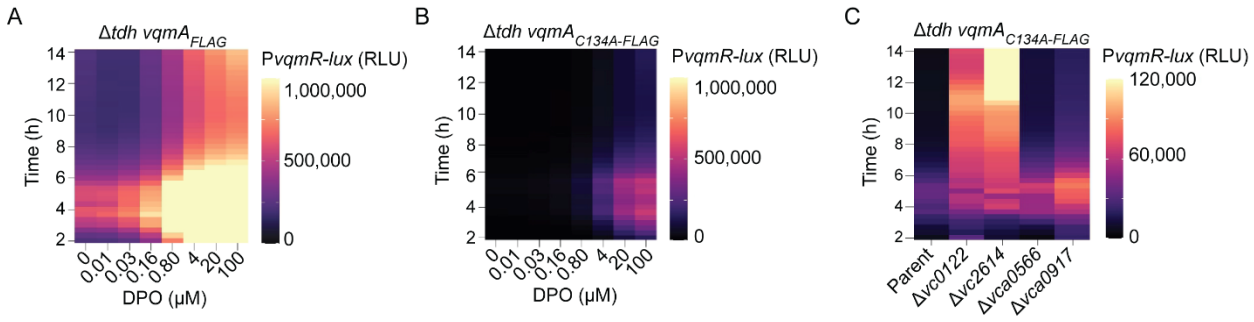

Figure 2. A genetic screen identifies repressors of the DPO-VqmA-VqmR QS circuit. (A) Light production over time from Δ*tdh vqmA*$_{FLAG}$ P*vqmR-lux* and (B) Δ*tdh vqmA*$_{C134A\text{-}FLAG}$ P*vqmR-lux V. cholerae* strains following administration of the specified concentrations of DPO. (C) As in panel B in the strain containing the additional designated deletions. DPO was added at 10 μM. Maximum fold-changes relative to that in the parent for Δ*vc0122*, Δ*vc2614*, Δ*vca0566*, and Δ*vca0917* were 9-fold at 11 h, 13.5-fold at 11 h 20 min, 2.8-fold at 17 h, and 3.3-fold at 14 h, respectively. RLU denotes relative light units, which are bioluminescence per OD_{600}. Scale bars represent color:intensity. Also see Supplementary Figure S1.

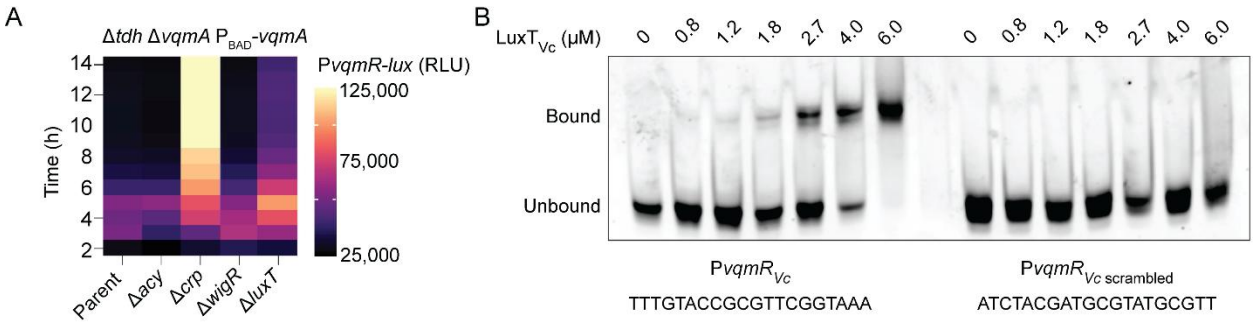

Figure 3. LuxT represses *vqmR* transcription. (A) Transcriptional output over time from P*vqmR-lux* following introduction of the indicated gene deletions in the Δ*tdh* Δ*vqmA* P_{BAD}-*vqmA V. cholerae* strain carrying P*vqmR-lux*. Maximum fold changes relative to the parent of the Δ*crp* and Δ*luxT* strains were 13.2-fold at 10 h and 2.5-fold at 8 h 20 min, respectively. RLU and scale bar as in Figure 2. (B) EMSA showing 6X-His-$LuxT_{Vc}$ (designated $LuxT_{Vc}$) binding to a P$vqmR_{Vc}$ probe (-111 to +49 relative to the $vqmR_{Vc}$ transcriptional start site) and the same probe with the putative LuxT binding site scrambled (P$vqmR_{Vc\ scrambled}$). The 20-nucleotide motif and its scrambled version are shown. All lanes contained 15 ng of promoter DNA. Bound and unbound DNA probes are designated.

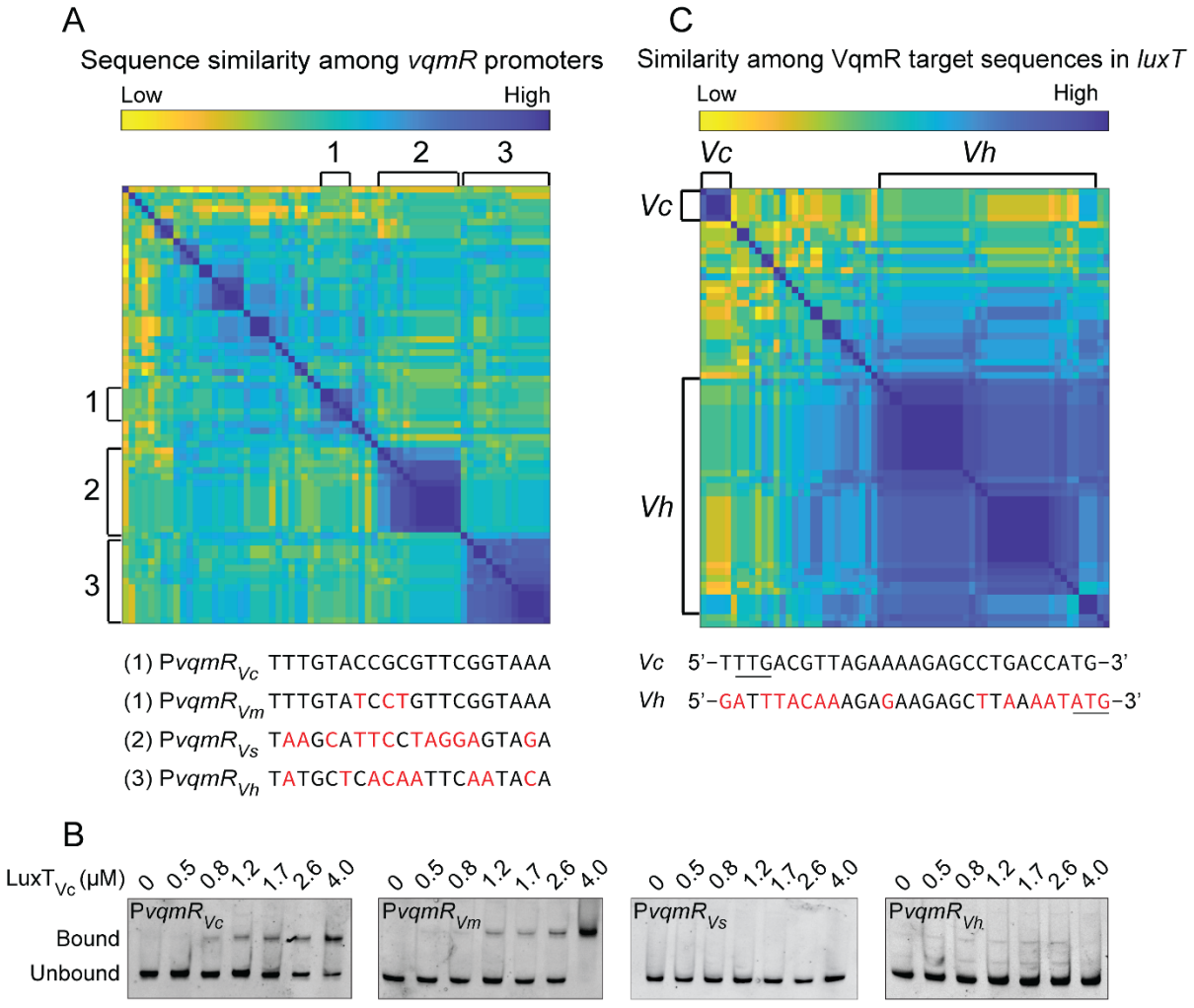

Figure 4. LuxT binds P*vqmR* in *V. cholerae* and in its close relative *V. metoecus*, but not P*vqmR* in more distantly related vibrios. (A) Pair-wise sequence similarity color-map of *vqmR* promoter regions from one representative genome from sixty-three vibrio species that harbor both *luxT* and *vqmR*. Hierarchical clustering was performed using the UPGMA algorithm (Unweighted Pair Group Methods with Arithmetic Mean). Putative LuxT binding sites for the designated groups are displayed below the heatmap with red indicating differences from the *V. cholerae* sequence. (B) EMSA of 6X-His-LuxT$_{Vc}$ (designated LuxT$_{Vc}$) binding to P*vqmR* DNA probes, similar in length to that in Figure 3B, containing putative LuxT binding sequences from *V. cholerae* (P*vqmR*$_{Vc}$), *V. metoecus* (P*vqmR*$_{Vm}$), *V. splendidus* (P*vqmR*$_{Vs}$), and *V. harveyi* (P*vqmR*$_{Vh}$). (C) Heatmap showing pair-wise sequence similarity of the *vqmR* target sites in the *luxT* transcript across the same

genomes as in panel A. Hierarchical clustering was performed using the UPGMA algorithm. A *V. cholerae*-like group (*Vc*) and a *V. harveyi*-like group (*Vh*) are highlighted, with representative sequences from each group shown below the heatmap. Red indicates differences from the *V. cholerae* sequence. The predicted TTG (*V. cholerae*) and ATG (*V. harveyi*) start codons are underlined.

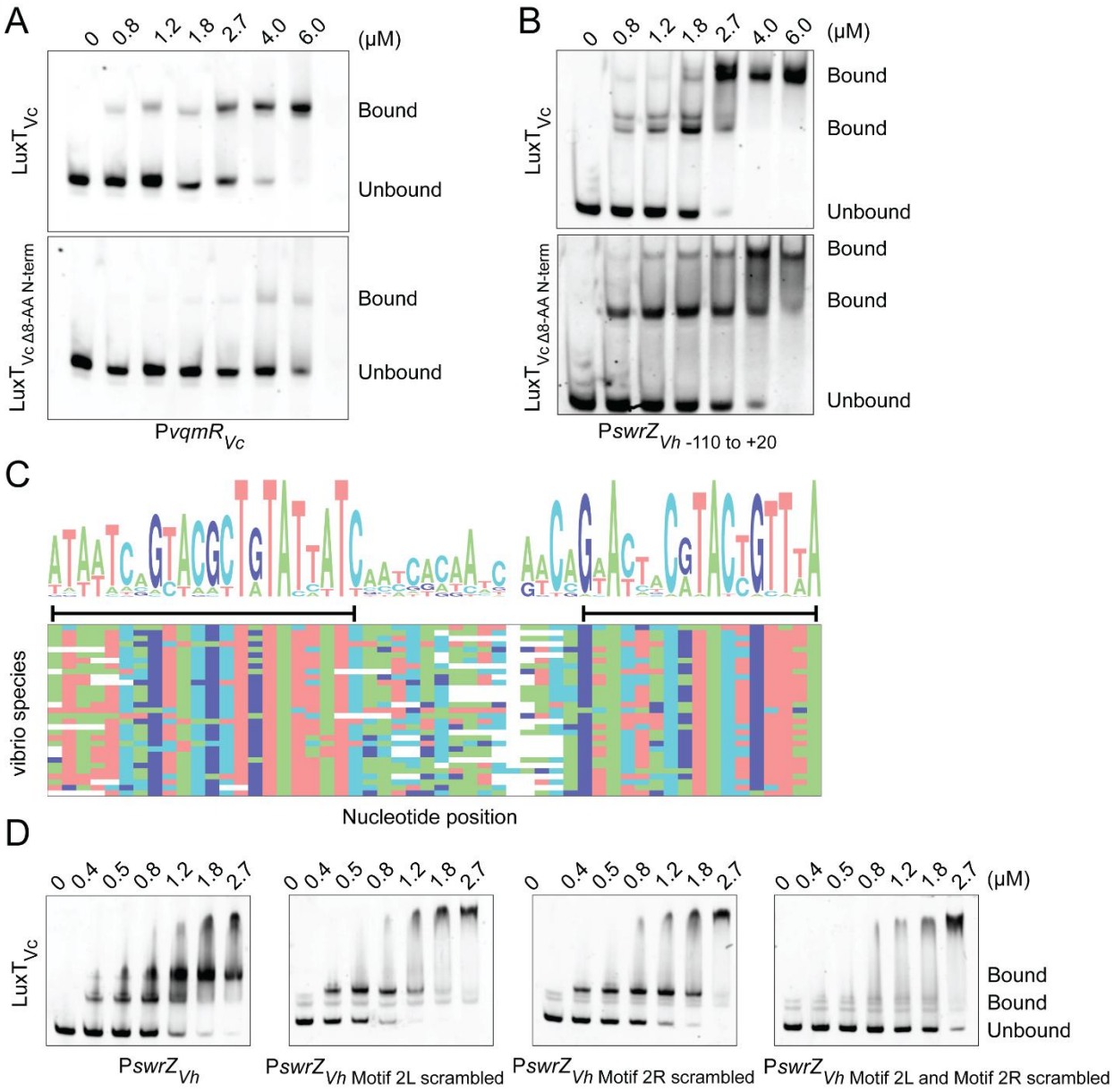

Figure 5. LuxT$_{Vc}$ binds distinct motifs in P*vqmR*$_{Vc}$ and P*swrZ*$_{Vh}$ and the 8 N-terminal amino acids in LuxT govern which sequence is bound. (A, B) EMSA analyses for 6X-His-LuxT$_{Vc}$ and 6X-His-LuxT$_{Vc\ \Delta 8\text{-AA N-term}}$ (denoted LuxT$_{Vc}$ and LuxT$_{Vc\ \Delta 8\text{-AA N-term}}$, respectively) binding to the P*vqmR*$_{Vc}$ probe DNA or to the *V. harveyi* P*swrZ*$_{Vh}$ -110 to +20 probe. (C) Heatmap showing a multi-sequence alignment of P*swrZ*$_{Vh}$ sequences across vibrio species. The consensus sequence logo is shown on top, with taller letters indicating higher conservation. The nucleotide-level alignment is provided in Supplementary Figure 9. The two conserved sequences, shown by the black bars underneath, differ by four bps

and are designated Motif 2L (for Left) and Motif 2R (for Right). DNA sequences for Motif 2L and Motif 2R are provided in Supplemental Figure 10. (D) EMSA analyses for $LuxT_{Vc}$ binding to the designated *V. harveyi* P*swrZ*$_{Vh}$ regions. Leftmost panel: the probe spans -110 to +20 and contains Motif 2L and Motif 2R sequences. In the three right panels, the -110 to +20 probe has one or both of Motif 2L and Motif 2R scrambled, as designated. Supplementary Figure S11 shows EMSAs for *V. harveyi* LuxT binding to the same fragments.

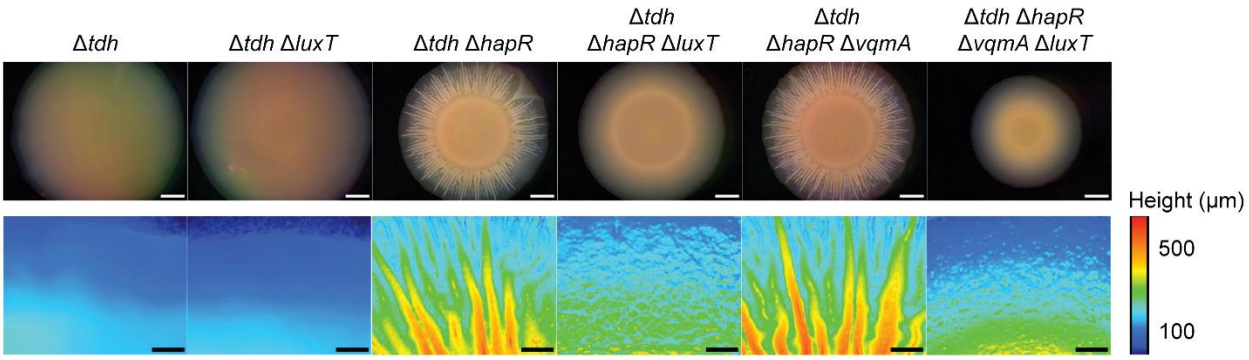

Figure 6. LuxT$_{Vc}$ promotes *V. cholerae* colony biofilm formation. Representative images of biofilms formed by the designated *V. cholerae* strains and companion quantitative 3D colony height profiles after 4 d. Height profiles are color mapped according to the scale provided.

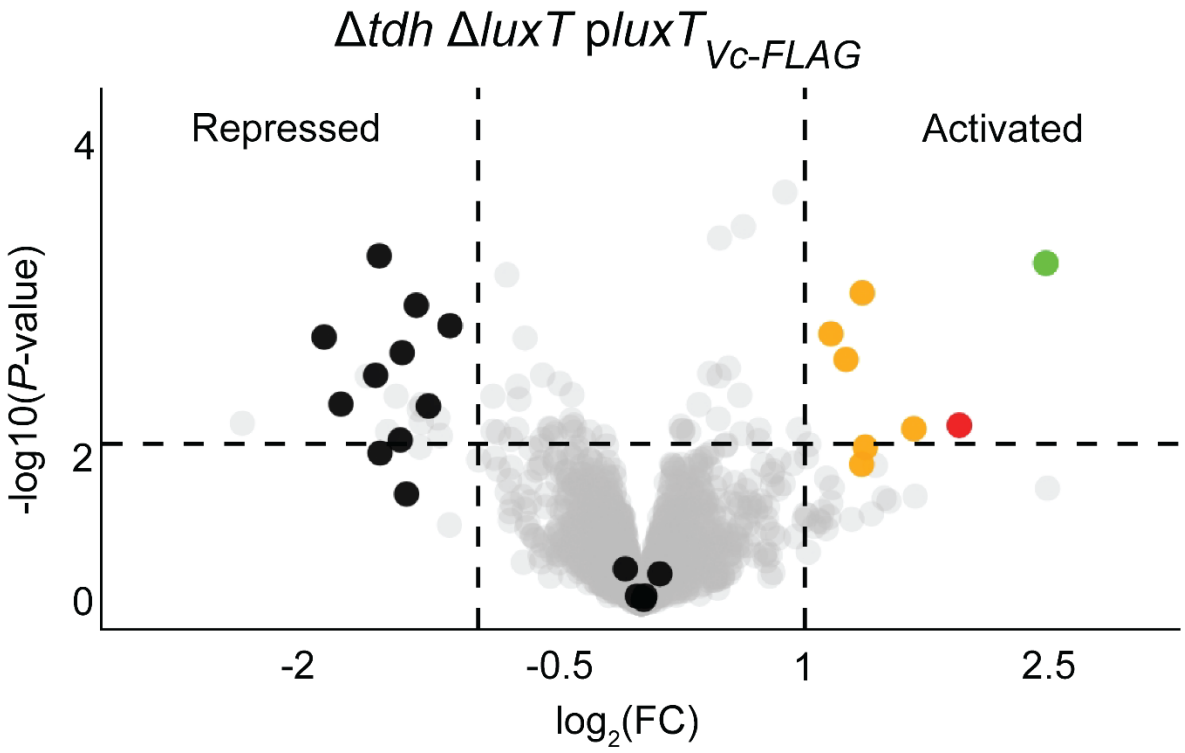

Figure 7. Transcriptomic analyses reveal the *V. cholerae* $LuxT_{Vc}$-controlled regulon. Volcano plot displaying gene expression patterns in the Δ*tdh* Δ*luxT V. cholerae* strain carrying $luxT_{Vc}$ expressed from an arabinose inducible promoter with 0.1% arabinose (p-P_{BAD}-$luxT_{Vc\text{-}FLAG}$. Sulfate metabolism genes are highlighted in black, galactose metabolism genes in orange, *vc1088* in red, and *luxT* in green. Data represent fold-changes for the indicated strain grown with 0.1% arabinose compared to the no arabinose condition. Genes repressed and activated by LuxT are denoted. The horizontal dotted line represents a P-value of 0.05. Left and right vertical dotted lines represent log_2 fold-changes of −1 and 1, respectively. Samples are from n = 3 biological replicates. Complete datasets are provided in Dataset S1.